

Error of semiclassical eigenvalues in the semiclassical limit - An asymptotic analysis of the Sinai billiard

Per Dahlqvist
Mechanics Department
Royal Institute of Technology, S-100 44 Stockholm, Sweden

Abstract

We estimate the error in the semiclassical trace formula for the Sinai billiard under the assumption that the largest source of error is due to Penumbra diffraction, that is diffraction effects for trajectories passing within a distance $R \cdot O((kR)^{-2/3})$ to the disk and trajectories being scattered in very forward directions. Here k is the momentum and R the radius of the scatterer. The semiclassical error is estimated by perturbing the Berry-Keating formula. The analysis necessitates an asymptotic analysis of very long periodic orbits. This is obtained within an approximation originally due to Baladi Eckmann and Ruelle. We find that the average error, for sufficiently large value of kR , will exceed the mean level spacing.

1 Introduction

During the early days of the trace formula nobody really believed that it could be used to predict individual eigenvalues, at least not in the strict semiclassical limit. There are mainly two (related) sources of errors. First, the semiclassical energy domain Green function is obtained by Laplace transforming the Van-Vleck propagator [1]. However, quantum evolution follows classical evolution only for a limited time, a time that seems to be longer than first expected [2], but still limited. Computing the Laplace transform (with time going from zero to infinity) of such an object is of course adventurous.

Secondly, the trace formula is obtained by taking the trace of this energy domain Green function by stationary phase technique. This is the procedure that selects out the periodic orbits. Whether or not this stationary phase approximation is justified for a particular cycle depends on \hbar , for sufficiently small \hbar it is always justified. So, the performance of the trace formula depends on the set of cycles that are required to resolve a particular state, and the accuracy of their semiclassical weights.

Consequently, the *semiclassical error* depends on the context, the method by which the eigenvalues are extracted. In the Berry-Keating method[3] it depends only on the error of the amplitudes of periodic orbits up to certain length, whereas in complex methods, based on *cycle expansions* [4], the error of the long cycles effects the convergence of the cycle expansion and the final position of the eigenvalue. An alternative approach

is based on the boundary integral method and the semiclassical limit of the characteristic determinant[5]. Bogomolny's transfer matrix method is closely related to this approach[6].

However, it turned out from, numerical computations that the Gutzwiller-Voros zeta function does exhibit complex zeroes quite close to the (real) quantum eigenvalues, at least in the lower part of the spectrum[7, 8, 9]. The Berry-Keating formula performed even better[9, 10]. This approach is based on a functional equation for the (exact) spectral determinant. By insisting on using the functional equation in the semiclassical limit, one actually put in information into the computation: *the spectrum is real*. The result may be a quite respective number of eigenvalues, only a few percent wrong.

None of these computations indicated what will happen in the strict semiclassical limit. Common estimates have suggested that the semiclassical errors, measured relative the mean level spacing, should tend to a constant as $\hbar \rightarrow \infty$, for system in two degrees of freedom. For a nice review, see ref [11].

Two common features of chaotic systems may cause problems to the stationary phase approximation. The first is intermittency. From a periodic point of view, it means that long orbits does not need to be very unstable, or more precisely, periodic orbit stabilities cannot be exponentially bounded with their length. If a long cycle is "relatively stable" it means that the corresponding saddle point is not isolated enough from its surroundings.

Secondly, the complex topology of generic systems make bifurcations abundant (with respect to variation of some parameter). So, for a generic systems there are "almost existing" and "almost forbidden" orbits all over phase space. For billiards the trace integral scans a function sprinkled with discontinuities. Nearly pruned orbits live near such discontinuities and the saddle point integrals has to be provided with cutoffs which leads to diffraction effects. Even Axiom-A systems such as the Baker map [12] suffers from diffraction effects but to a less extent. For smooth potentials one has to face stabilization of cycles close to bifurcation. Sufficiently pruned orbits can be included as ghost orbits [13] but close to bifurcations uniform approximations has to be invoked[14, 15].

There are two pioneering studies indicating that many of the terms included in the Berry-Keating sum are way off, the stationary phase approximation behind them is simply not justified. Tanner [16] studied the dynamics close to the bouncing ball orbit in the stadium billiard, and Primack et.al. [17] studied the Sinai billiard and orbits scattering in very forward direction or sneaking very close to the disk. Both cases deals with systems with neutral orbits and as such intermittent.

The paper [17] by Primack et.al. is the main inspiration for the present study. By estimating the size of this *penumbra* and its scaling in energy, they concluded that "*the semiclassical approximation fails for the majority of the relevant PO's (periodic orbits) in the semiclassical limit*". It thus seems likely that the Berry-Keating approach will eventually cease to produce individual eigenvalues. Such a conclusion is by no means obvious. Simple conclusions can (maybe) be drawn if the system is uniformly hyperbolic. But cycles contribute with very different weights in intermittent systems, such as the Sinai billiard. If a minority of non diffractive cycles carried a large part of the semiclassical weight one could perhaps argue that the trace formula could be saved. But unfortunately the situations is the opposite. The cycles being most prone to penumbra diffraction have

large semiclassical weights. The goal of this paper is to make this reasoning more precise.

In a latter study Primack et.al. [11] seems to tone down the importance of Penumbra diffraction. They suggest that the semiclassical error in the semiclassical limit is of the order of the mean level spacing, or at most diverges logarithmically. It could thus be possible to resolve individual states even in the strict semiclassical limit. The study is mainly numerical, it is an ambiguous attempt to extrapolate from finite sets of quantum states and periodic orbits into the semiclassical limit. Our present study will not support their claims. We will indeed find that the error will irrevocably increase beyond the mean level spacing.

It is evident that a numerical study of the semiclassical error with periodic orbits is, least to say, difficult. A central tool in our approach will be asymptotic theory for the sets of periodic orbits based on an idea of Baladi Eckmann and Ruelle [18, 19, 20, 21, 22].

What we do is a model study of an intermittent system in two degrees of freedom. One should of course be cautious when trying to generalize the result to other system, especially to hyperbolic ones. The trace formula is indeed exact for some hyperbolic system, such as the Cat map [23, 24] and geodesic flow on surfaces of constant negative curvature [25]. The trace formula will probably perform much better in the hyperbolic case than in the intermittent.

The disposition of the article is very much like a cooking recipe. In section 2 we present all the ingredients, such as the semiclassical zeta function, the Berry-Keating formula, penumbra diffraction, some classical periodic orbit theory and the BER approximation. In sec. 3 we do the actual cooking. We consider the shift of a zero of the Berry-Keating formula if a perturbation, due to an error, is added. This simple exercise gives us the semiclassical error in terms of finite sums over pseudo orbits. We then relate these pseudo orbit sums to various zeta functions. These zeta functions are then calculated in the asymptotic theory which we call the BER approximation. In section 4 we present the outcome of these exercises. Then follows (section 5) a round table discussion about the validity of the various assumptions and approximations that underlies the results.

2 Ingredients

2.1 The semiclassical zeta function

The starting point will be the Gutzwiller-Voros zeta function [1] whose zeros is to be associated with the quantum eigenvalues. It is represented as a product over all primitive periodic orbits p of the systems.

$$Z^{sc}(E) = \prod_p \prod_{m=0}^{\infty} \left(1 - \frac{e^{i[S_p/\hbar - \mu_p \frac{\pi}{2}]} }{|\Lambda_p|^{1/2} \Lambda_p^m} \right) . \quad (1)$$

where S_p is the action along p , μ_p the Maslov index and Λ_p is the expanding eigenvalue of the Jacobian. To turn this into a Dirichlet series one first expand the inner Euler-

product

$$Z^{sc}(E) = \prod_p \sum_{n=0}^{\infty} \frac{\Lambda_p^{-n(n-1)/2}}{\prod_{j=1}^n (1 - \Lambda_p^{-j})} \left(-\frac{e^{i[S_p/\hbar - \mu_p \frac{\pi}{2}]}}{|\Lambda_p|^{1/2}} \right)^n \quad (2)$$

$$= \prod_p \sum_{n=0}^{\infty} C_{p,n} e^{i[nS_p - n\mu_p \frac{\pi}{2}]} \quad (3)$$

where

$$C_{p,n} = (-1)^n \frac{\Lambda_p^{-n(n-1)/2}}{|\Lambda_p|^{n/2} \prod_{j=1}^n (1 - \Lambda_p^{-j})} \quad (4)$$

If we now expand the product over p , we obtain a *cycle expansion* [27] - a sum over all pseudo-orbits, that is all distinct combinations of periodic orbits: $\alpha = p_1^{n_{p_1}} p_2^{n_{p_2}} \dots p_k^{n_{p_k}} \dots$

$$Z^{sc}(E) = \sum_{\alpha} C_{\alpha} e^{i[S_{\alpha} - \mu_{\alpha} \frac{\pi}{2}]} \quad (5)$$

where we have defined the quantities

$$C_{\alpha} = \prod_p C_{p,n_p} \quad (6)$$

$$S_{\alpha} = \sum_p n_p S_p \quad (7)$$

$$\mu_{\alpha} = \sum_p n_p \mu_p \quad (8)$$

We will restrict ourselves to billiards, the cycle action S_p is then given in terms of the geometric length $S_p = L_p \cdot k$ where $k = \sqrt{2E}$. The units are chosen such that $m = \hbar = 1$ and the semiclassical limit $\hbar \rightarrow 0$ is replaced by $k \rightarrow \infty$. In the following we absorb the maslov indices in the amplitudes C_{α}

$$Z^{sc}(k) = \sum_{\alpha} C_{\alpha} e^{iL_{\alpha}k} \quad (9)$$

Since we are considering billiards, the redefined amplitudes C_{α} will still be real.

Note that the size of the amplitudes is

$$C_{p,n} \sim \frac{1}{|\Lambda|^{n^2/2}} \quad (10)$$

to leading order, and thus decays fast with n . The zeta function is not seriously affected if one restricts the n 's to $n \in \{0, 1\}$. This amounts to retain only the factor $m = 0$ in (1). The resulting type of zeta function is often referred to as a *dynamical zeta function*.

2.2 The Berry-Keating formula

The spectral determinant for a billiard obeys the functional equation

$$D(k) = D(-k) \quad . \quad (11)$$

The semiclassical analogue to the spectral determinant is

$$D^{sc}(k) = e^{-i\pi\bar{N}(k)} Z^{sc}(k) = \sum_{\alpha} C_{\alpha} e^{i(L_{\alpha}k - \pi\bar{N}(k))} \quad (12)$$

The idea of Berry and Keating [3] was to postulate that this semiclassical determinant also satisfies the functional equation (11). This is of course not exactly true ¹ but by insisting on it one can convert eq. (12) to a finite sum

$$D^{sc}(k) = 2 \sum_{\alpha: L_{\alpha} < L_{BK}} C_{\alpha} \cos(L_{\alpha}k - \pi\bar{N}(k)) \quad (13)$$

where

$$L_{BK} = \pi \frac{d\bar{N}(k)}{dk} \quad . \quad (14)$$

$\bar{N}(k)$ is the mean spectral staircase function. For a billiard it is, to leading order, given by

$$\bar{N} = \frac{Ak^2}{4\pi} \quad , \quad (15)$$

where A is the billiard area. So the cutoff length is given by

$$L_{BK} = \frac{Ak}{2} \quad (16)$$

If neutral orbits are present, and they are in the Sinai billiard, their contribution can be included in $\bar{N}(k)$ which is then decorated by oscillation whose amplitude decreases with increasing k .

2.3 The classical zeta function

Another central object in our investigation will be the (weighted) evolution operator[27], whose action on a phase space distribution function $\Phi(x)$ is given by

$$\mathcal{L}_w^t \Phi(x) = \int w(x, t) \delta(x - f^t(y)) \Phi(y) dy \quad . \quad (17)$$

The phase space point x is taken by the flow to $f^t(x)$ during time t . $w(x, t)$ is a weight associated with a trajectory starting at x and evolved during time t . It is multiplicative along the flow, that is $w(x, t_1 + t_2) = w(x, t_1)w(f^{t_1}(x), t_2)$. If $w \equiv 1$, the operator just describes the classical evolution of the phase space density.

¹In e.g. the Sinai billiard the semiclassical zeta function has a branch cut along the negative imaginary k -axis and the equation $D^{sc}(k) = D^{sc}(-k)$ cannot hold [26]

In the following we will restrict ourselves to chaotic 2-D billiards, and will use traversed length L as 'time' variable.

The trace of this operator can be represented in terms of periodic orbits in two ways. First as a sum

$$\text{tr} \mathcal{L}_w^L = \sum_p L_p \sum_{r=1}^{\infty} w_p^r \frac{\delta(L - rL_p)}{|\det(1 - M_p^r)|} , \quad (18)$$

where r is the number of repetitions of primitive orbit p , having period L_p , and M_p is the Jacobian of the Poincaré map, its expanding eigenvalue is Λ_p and w_p is the weight associated with cycle p .

The trace can also be written in terms of a *zeta function* or *Fredholm determinant*:

$$\text{tr} \mathcal{L}_w^L = \frac{1}{2\pi i} \int_{a-i\infty}^{a+i\infty} e^{sL} \frac{Z'_w(s)}{Z_w(s)} ds . \quad (19)$$

The classical zeta function $Z_w(s)$ is given by

$$Z_w(s) = \prod_p \prod_{m=0}^{\infty} \left(1 - w_p \frac{e^{-sL_p}}{|\Lambda_p| \Lambda_p^m} \right)^{m+1} . \quad (20)$$

Again we suffice with the $m = 0$ factors, and define instead the classical zeta function as

$$Z_w(s) = \prod_p \left(1 - w_p \frac{e^{-sL_p}}{|\Lambda_p|} \right) . \quad (21)$$

In case the zeta function is entire, the trace can be written as a sum over zeros s_γ of the zeta function

$$\text{tr} \mathcal{L}_w^L = \sum_{\gamma} e^{s_\gamma L} , \quad (22)$$

where $e^{s_\gamma L}$ can be interpreted as the eigenvalues of the evolution operator. Precisely as the semiclassical zeta function, the classical zeta function $Z_w(s)$ can be subject to a cycle expansion

$$Z_w(s) = \sum_{\alpha} a_{\alpha}(w) e^{-sL_{\alpha}} . \quad (23)$$

We will eventually use the weight $w(x, L)$ to account for diffraction but for the time being it is just an arbitrary weight.

2.4 The BER approximation

We note that the identity in sec 2.3, holds also after smearing,

$$\text{tr} \mathcal{L}_{\sigma}^L = \sum_p L_p \sum_{r=1}^{\infty} w_p^r \frac{\delta_{\sigma}(L - rL_p)}{|\det(1 - M_p^r)|} = \frac{1}{2\pi i} \int_{a-i\infty}^{a+i\infty} e^{sL} \frac{Z'_w(s)}{Z_w(s)} e^{(is\sigma)^2/2} ds \quad (24)$$

where $\delta_{\sigma}(\cdot)$ are gaussians of standard deviation σ . We will be interested in very gross features of periodic sums. Such information is encoded in the behavior of the zeta function

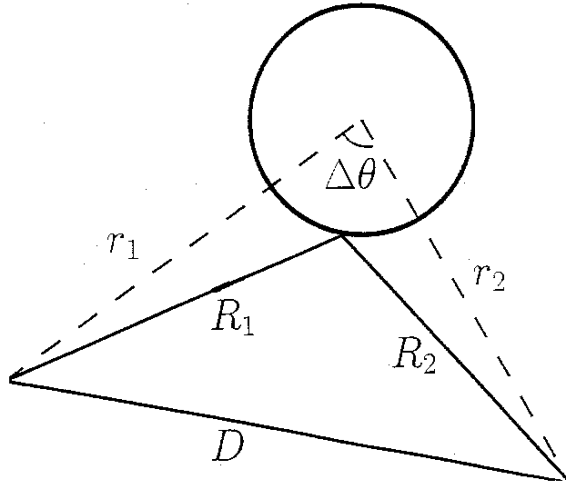


Figure 1: Some notations used in the discussion of the one-disk Green function.

for small s and can be estimated by the Baladi-Eckmann-Ruelle (BER) approximation [18]. The probabilistic approach that underlies this approximation has a long history, see eg [28]. It was put into the context of Ruelle resonances by Baladi, Eckmann and Ruelle in [18]. In [19, 20, 21, 22] the formalism was generalized to include zeta functions with general thermodynamic weights, and the evaluation of chaotic averages.

Intermittent systems fluctuate between chaotic and quasi regular behavior. The basic idea is to define a surface of section such that all trajectories from the section back to itself traverse a chaotic region at least once. The coordinate on this surface of section will be denoted x_s .

Let $\Delta_s(x_s)$ the length of a trajectory starting at x_s and back to the surface of section. Further, let $w(x_s)$ be the weight integrated along this segment. We define the (weighted) distribution of recurrence time as

$$p_w(L) = \int w(x_s) \delta(L - \Delta_s(x_s)) dx_s \quad , \quad (25)$$

where we have assumed the measure dx_s to be normalized: $\int dx_s = 1$. The approximate zeta function is then given in terms of the Laplace transform of this function

$$Z(s) \approx \hat{Z}(s) = 1 - \int p_w(L) e^{-sL} dL \quad . \quad (26)$$

2.5 Penumbra diffraction

A convenient starting point for deriving the semiclassical trace formula for billiards, and to study its limitations, is the Boundary Integral Method [29, 17, 5]. The eigenvalues of

the problem are those for which the following integral equation has a solution

$$u(\mathbf{r}(s)) = 2 \int_S \frac{\partial G}{\partial \hat{n}_s}(\mathbf{r}(s), \mathbf{r}(s')) u(\mathbf{r}(s')) ds' . \quad (27)$$

The integral is performed along the boundary of the billiard. The function $u(\mathbf{r}(s))$ is related to the wave function according to the normal derivative

$$u(\mathbf{r}(s)) = \frac{\partial \Psi(\mathbf{r}(s))}{\partial \hat{n}_s} . \quad (28)$$

The boundary $\mathbf{r}(s)$ is parameterized by the Birkhoff coordinate s .

We can write eq (27) symbolically as a matrix equation

$$(\mathbf{I} - \mathbf{A})\mathbf{U} = 0 , \quad (29)$$

having a solution when $\det(\mathbf{I} - \mathbf{A}) = 0$. We can write this determinant as

$$\det(\mathbf{I} - \mathbf{A}) = e^{\text{tr} \log(\mathbf{I} - \mathbf{A})} = e^{-\sum_{n=1}^{\infty} \frac{1}{n} \text{tr}(\mathbf{A}^n)} , \quad (30)$$

where

$$\text{tr}(\mathbf{A}^n) = 2^n \int ds_1 \dots ds_n \frac{\partial G}{\partial \hat{n}_{s_1}}(\mathbf{r}(s_1), \mathbf{r}(s_2)) \dots \frac{\partial G}{\partial \hat{n}_{s_{n-1}}}(\mathbf{r}(s_{n-1}), \mathbf{r}(s_n)) \frac{\partial G}{\partial \hat{n}_{s_n}}(\mathbf{r}(s_n), \mathbf{r}(s_1)) . \quad (31)$$

There is considerable liberty of choosing the Green function $G(\mathbf{r}, \mathbf{r}')$. In order to study the problem of Penumbra diffraction Primack et.al [17] suggested to use the one disk Green function (see below) in (27). The integral in (27) need then be performed only along the square boundary.

The one disk Green function reads [30]

$$G(r_1, r_2, \Delta\theta) = \frac{i}{8} \sum_{\ell=-\infty}^{\infty} \left(H_{\ell}^{(2)}(kr_1) + S_{\ell}(kR) H_{\ell}^{(1)}(kr_1) \right) H_{\ell}^{(1)}(kr_2) e^{i\ell(\Delta\theta)} , \quad (32)$$

where $H_{\ell}^{(1)}(z)$ and $H_{\ell}^{(2)}(z)$ are Hankel functions and r_1 , r_2 and $\Delta\theta$ are explained in fig. 1. The phase shift function $S_{\ell}(kR)$ is defined by

$$S_{\ell}(kR) = -\frac{H_{\ell}^{(2)}(kR)}{H_{\ell}^{(1)}(kR)} . \quad (33)$$

Using Poisson resummation we get

$$G(r_1, r_2, \Delta\theta) = \sum_{m=-\infty}^{\infty} G^{(m)}(r_1, r_2, \Delta\theta) , \quad (34)$$

where

$$G^{(m)}(r_1, r_2, \Delta\theta) = \frac{i}{8} \int_{-\infty}^{\infty} \left(H_{\ell}^{(2)}(kr_1) + S_{\ell}(kR) H_{\ell}^{(1)}(kr_1) \right) H_{\ell}^{(1)}(kr_2) e^{i\ell(\Delta\theta + 2\pi m)} d\ell . \quad (35)$$

The standard semiclassical result is obtained if we

1. Retain only the integral approximation $G^{(m=0)}$ in (35) for the Green function, semiclassically this means that classically forbidden orbits such as creeping orbits are neglected.
2. Use the Debye approximations for the Hankel functions.
3. Compute the integrals by stationary phase. The term $\text{tr}(\mathbf{A}^n)$ in (31) will now contain contributions from all periodic orbits with n bounces on the square boundary.

In fig. 2 we plot the circle Green function together with its semiclassical limit. Semiclassically there is a discontinuity at $d = R$ (where d is the classical impact parameter) marking the transition between the lit region and the shadow. In the exact Green function there is of course a smooth transition. The interesting thing is that the exact result is suppressed as compared to the semiclassical within a distance d_{crit} , a destructive interference between the rays starts already in the lit region and continues into the classical shadow.

This twilight zone was called Penumbra in [17]. In appendix A we show that

$$d_{crit} = (1 + \epsilon_{max}(kR))R \quad , \quad (36)$$

with

$$\epsilon_{max}(kR) = c(kR)^{-2/3} \quad , \quad (37)$$

where c depend only weakly (logarithmically) on kR , r_1 , r_2 and R . The subscript *max* was used in the appendix but will be dropped from now on.

In the penumbra the usually semiclassical look of the Green function is lost. It is hard to foresee how what happens when this object is convoluted with itself a la eq. (31), in order to get contributions from periodic orbits doing several passages of the penumbra. To use the periodic orbit apparatus described in sec 2.3 we need a weight that is multiplicative along the flow. However, we will not use the cycles to actually compute the spectrum, we are only interested in estimating the error induced by penumbra diffraction, so we can suffice with a rather crude weight. Before we make up our mind how this should be achieved, let us discuss the periodic orbits in the Sinai billiard.

The cycles can be coded by associating a (coprime) lattice vector \mathbf{q} with each disk-to-disk segment, see sec. 3.3. In the limit of small R any such periodic sequence $p_t = \overline{\mathbf{q}_1 \mathbf{q}_2 \dots \mathbf{q}_n}$ can be realized in the system, except for the rule that two consecutive lattice vector may not be identical[20]. Suppose now that we increase the size R of the disk. Some segment of the periodic orbit, say \mathbf{q}_1 , would then eventually need to go through the disk which of course is prohibited, the cycle is then said to be pruned. Let's say that this happen when $R = R_{bif}$. For $R < R_{bif}$, there is another cycle $p_r = \overline{\mathbf{q}_{1a} \mathbf{q}_{1b} \mathbf{q}_2 \dots \mathbf{q}_n}$ that actually do scatter at the disk when the companion p_t just pass by. When $R = R_{bif}$, p_t and p_r overlap exactly and when $R > R_{bif}$ they are both pruned. This is an analogue of the saddle-node bifurcation in smooth potential, and the only source or pruning in the Sinai billiard. For a lucid discussion of pruning in billiards, see [31].

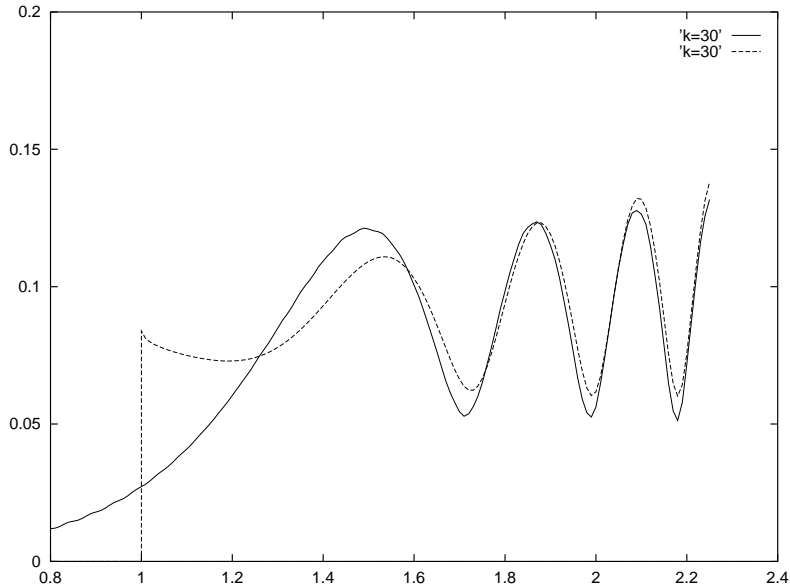


Figure 2: The circle Green function versus impact parameter d for fixed values of $k = 30$, $R = 1$ and $r_1 = r_2 = 3$. The full line represents the exact result and the dashed line the semiclassical approximation.

Obviously there is a close connection between pruning and penumbra diffraction. The semiclassical weights drops suddenly to zero when the pair is pruned. We have learned from our studies of the circle Green function that the quantum pruning is more gradual.

To estimate the error we will say the pair effectively annihilate each other if they are within the transition region discussed above. Note that since $|\Lambda_{pr}| \gg |\Lambda_{pt}|$, we need in practice only consider the removal of p_t .

So we define an cycle to be diffractive if it passes the disk within the distance ϵR (as given by (37)). The error of the semiclassical weight C_p for a diffractive cycle is thus defined as $\delta C_p = -C_p$. A pseudo orbit is diffractive if at least one of the participating prime cycles is diffractive. The error of the diffractive pseudo orbit's amplitude is thus $\delta C_\alpha = -C_\alpha$.

To exclude diffractive cycles from cycle sums we introduce a multiplicative cycle weight w_p such that $w_p = 0$ if the orbit is affected by diffraction and $w_p = 1$ if not. Exactly, how this is done is discussed in section 3. The associated pseudo cycle weight is

$$w_\alpha = \prod_p w_p^{n_p} . \quad (38)$$

(with the convention that $0^0 = 1$) where n_p is restricted to $n_p \leq 1$.

One can also consider families of cycles with n passages of the penumbra. For each passage the trajectory can either choose to bounce off the disk or not. So such a family thus consists of 2^n members and only one of them is unremoved from the calculation according to our rule above. This is the one bouncing at every passage of the penumbra,

the semiclassical weight of this one is of course very much suppressed and the neglect of this orbit is completely negligible.

The weight now depends on the parameter ϵ . We will skip the index w on the classical zeta function (21) and instead denote it $Z(s; \epsilon)$. Traces will be denoted $\text{tr} \mathcal{L}_\epsilon^L$ etc.

3 Preparation

3.1 Perturbation of the Berry-Keating zeros

Let k_0 be a zero of $D(k)$ as given by (13) (with superscript omitted):

$$D(k_0) = 2 \sum_{\alpha} C_{\alpha} \cos(L_{\alpha} k - i\pi \bar{N}(k)) = 0 \quad . \quad (39)$$

All pseudo orbit sums are hence forth subject to the cutoff $L_{\alpha} < L_{BK}$, which will not be explicitly written out in the sums.

We are interested in how small errors in the amplitudes C_{α} will effect the location of this zero. We thus add a small perturbation

$$\delta D(k) = 2 \sum_{\alpha} \delta C_{\alpha} \cos(L_{\alpha} k - i\pi \bar{N}(k)) \quad , \quad (40)$$

where δC_{α} is the error of C_{α} , and try to solve

$$D(k) + \delta D(k) = 0 \quad . \quad (41)$$

We then expand $k = k_0 + \delta k$ and consider the solution to

$$D'(k_0) \delta k + \delta D(k_0) + \delta D'(k_0) \delta k = 0 \quad . \quad (42)$$

We neglect the last term, it provide higher order corrections and get

$$\delta k = - \frac{\delta D(k_0)}{D'(k_0)} \quad . \quad (43)$$

We will consider the perturbation of a typical zero, sitting at a distance $\sim \bar{d}^{-1}$ (where $\bar{d} = \frac{d\bar{N}}{dk}$) from the neighboring zeros. If we assume that the oscillations of $D(k)$ are sine-like we can relate the derivative at a typical zero $D'(k_0)$ to the mean square of the determinant

$$D'(k_0) = \bar{d} \sqrt{2\pi^2 \langle D(k_0)^2 \rangle} \quad . \quad (44)$$

We then get for the mean square of the shift

$$\langle \delta k^2 \rangle^{1/2} = \bar{d}^{-1} \left(\frac{\langle \delta D(k_0)^2 \rangle}{2\pi^2 \langle D(k_0)^2 \rangle} \right)^{1/2} \quad . \quad (45)$$

First we focus on the denominator of eq. (45). We obtain

$$\langle D(k_0)^2 \rangle = \frac{1}{2} 2^2 \sum_{\alpha} C_{\alpha}^2 \quad , \quad (46)$$

assuming that cross terms cancel out, cf section 5.3.

The average perturbation is, by the same arguments, given by

$$\langle \delta D^2(k_0) \rangle = 2 \sum_{\alpha} \delta C_{\alpha}^2 \quad , \quad (47)$$

and

$$\langle \delta k^2 \rangle^{1/2} = \left(\frac{\sum_{\alpha} \delta C_{\alpha}^2}{\sum_{\alpha} C_{\alpha}^2} \right)^{1/2} \bar{d}^{-1} / \sqrt{2\pi^2} \equiv F(k_0) \bar{d}^{-1} / \sqrt{2\pi^2} \quad . \quad (48)$$

Following our reasoning in sec 2.5 we put

$$\delta C_{\alpha}^2 = (1 - w_{\alpha}) C_{\alpha}^2 \quad . \quad (49)$$

Recall that w_{α} is either 0 or 1. We can rewrite the function F as

$$F(k_0) = \left(1 - \frac{\sum_{\alpha} w_{\alpha} C_{\alpha}^2}{\sum_{\alpha} C_{\alpha}^2} \right)^{1/2} \quad . \quad (50)$$

Recall that we are only considering pseudo orbits such that $n_p \leq 1$ so

$$|C_{\alpha=p_1 p_2 \dots p_k}|^2 = |\Lambda_{\alpha}|^{-1} \equiv |\Lambda_{p_1} \cdot \Lambda_{p_1} \dots \Lambda_{p_k}|^{-1} \quad . \quad (51)$$

We can now rewrite the numerator and denominator of (50) in terms of the classical weights $a(\epsilon)$ introduced in section 2.3

$$\sum_{\alpha} w_{\alpha}(\epsilon) C_{\alpha}^2 = \sum_{\alpha} |a_{\alpha}(\epsilon)| \quad (52)$$

$$\sum_{\alpha} C_{\alpha}^2 = \sum_{\alpha} |a_{\alpha}(0)| \quad . \quad (53)$$

The perturbative approach taken in this section is only valid if the predicted value of F is small. If F approaches unity there is no other interpretation than a failure of the Berry-Keating formula to resolve individual states.

3.2 Treating the pseudo orbit sums

The goal of this section is to relate the pseudo orbit sums (52) and (53) to various zeta functions. There is an important distinction between these pseudo orbits sums and the cycle expansion (23) - the occurrence of the absolute values in eqs. (52) and (53). To deal with this we will borrow a trick from ref. [32].

Consider the classical zeta function (that is eq. (21) with higher m factors omitted)

$$Z(s; \epsilon) = \prod_p (1 - w_p(\epsilon) \frac{e^{-sL_p}}{|\Lambda_p|}) \quad . \quad (54)$$

Consider the cycle expansion of a derived zeta function (note the plus-sign!)

$$Z^+(s; \epsilon) = \prod_p (1 + w_p(\epsilon) \frac{e^{-sL_p}}{|\Lambda_p|}) = \sum_{\alpha} b_{\alpha}(\epsilon) e^{-sL_{\alpha}} \quad (55)$$

All b_α are positive, in fact, they are the summands of eqs (52) and (52)

$$b_\alpha(\epsilon) = |a_\alpha(\epsilon)| \quad , \quad (56)$$

We rewrite this as

$$Z^+(s; \epsilon) = \int_0^\infty b(L; \epsilon) e^{-sL} dL \quad (57)$$

where

$$b(L; \epsilon) = \sum_\alpha b_\alpha \delta(L - L_\alpha) \quad . \quad (58)$$

Conversely, the function $b(L; \epsilon)$ is related to the zeta function by means of an inverse Laplace transform

$$b(L; \epsilon) = \frac{1}{2\pi i} \int_{\sigma-i\infty}^{\sigma+i\infty} Z^+(s; \epsilon) e^{sL} ds \quad . \quad (59)$$

The semiclassical error can now be written in terms of the function $b(L; \epsilon)$

$$F = \sqrt{1 - \frac{\int_0^{L_{BK}} b(L; \epsilon) dL}{\int_0^{L_{BK}} b(L; 0) dL}} \quad (60)$$

where L_{BK} is given by eq. (14) and ϵ is given eq. (37).

If we now define yet another zeta function

$$Z_2(s; \epsilon) = \prod_p (1 - w_p^2 \frac{e^{-2sL_p}}{|\Lambda_p|^2}) \quad (61)$$

we can rewrite $Z^+(s; \epsilon)$ as

$$Z^+(s; \epsilon) = \frac{Z_2(s; \epsilon)}{Z(s; \epsilon)} \quad . \quad (62)$$

If the involved zeta functions are entire we can write

$$b(L; \epsilon) = \sum_\gamma \text{res} \frac{Z_2(s; \epsilon)}{Z(s; \epsilon)} \Big|_{s=s_\gamma} e^{s_\gamma L} \quad (63)$$

which should be compared with (22). The asymptotic behavior of $b(L; \epsilon)$ is (under much milder assumptions on the analytic properties) related to the leading zero $s_0(\epsilon)$

$$b(L; \epsilon) \sim \text{res} \frac{Z_2(s; \epsilon)}{Z(s; \epsilon)} \Big|_{s=s_0} e^{s_0 L} = \frac{Z_2(s_0(\epsilon); \epsilon)}{Z'(s_0(\epsilon); \epsilon)} e^{s_0 L} \quad (64)$$

This leading asymptotic behavior is all we need to evaluate the integrals in eq. (60) since we are interested in the asymptotics of the function F . Moreover, as discussed in section 2.4, the behavior of zeta functions close to the origin is insensitive to fine details in the spectrum of periodic orbits, a theory for the large scale structure of periodic orbits exist and will be worked out in detail in the next section.

3.3 Implementing the BER approximation for the Sinai billiard

The BER approximation is very well suited for the Sinai billiard, in particular if the scatterer is small. The obvious choice of the surface of section is provided by the disk itself [20].

Consider now the unfolded representation of the Sinai billiard. A trajectory segment from the disk to itself can thus be considered as going from one disk, associated with lattice vector $(0, 0)$ to some other disk represented by lattice vector \mathbf{q} . All segments going to \mathbf{q} have essentially the same length $q = |\mathbf{q}|$ and the following simple expression for the distribution of recurrence lengths will suffice for our purposes.

$$p(L; \epsilon) = \sum_{\mathbf{q}} \hat{a}_{\mathbf{q}}(\epsilon) \delta(L - q) \quad , \quad (65)$$

where

$$\hat{a}_{\mathbf{q}}(\epsilon) = \int_{\Omega_q} w(x_s) dx_s \quad . \quad (66)$$

Ω_q is the set of initial points x_s whose target is \mathbf{q} . The approximate zeta function is then

$$\hat{Z}(s; \epsilon) = 1 - \int_0^\infty p(L; \epsilon) e^{-sL} ds = 1 - \sum_{\mathbf{q}} \hat{a}_{\mathbf{q}}(\epsilon) e^{-sq} \quad . \quad (67)$$

The weight, as defined in sec. 2.5 will be zero, $w(x_s) = 0$, if the trajectory starting at x_s and heading for disk \mathbf{q} pass some other disk within a distance ϵR before actually hitting \mathbf{q} , otherwise it is equal one, $w(x_s) = 1$.

If $\epsilon = 0$, then $\hat{a}_{\mathbf{q}}$ is the phase space area corresponding to disk \mathbf{q} .

The computation of $p(L; \epsilon)$ will unfortunately be long and boring. It will run in parallel with ref [33] in large parts and we will frequently refer to that paper. All error estimates in [33] carry over directly, so we will simply omit them below to make things a little more transparent. Nevertheless, we will without hesitation display equations as strict equalities, but the reader should bear in mind that all expressions are valid in the small R limit.

Consider now a trajectory hitting disk \mathbf{q} . The relation between the phase space variables ϕ and α , see fig 3, and the scattering angle $\beta_{\mathbf{q}}$ on disk \mathbf{q} is given by

$$R_{\mathbf{q}} \sin \beta_{\mathbf{q}} - R \sin \alpha = q \sin(\phi - \theta_{\mathbf{q}} - \alpha) \quad , \quad (68)$$

where $\theta_{\mathbf{q}}$ is the polar angle of the lattice vector \mathbf{q} , and $R_{\mathbf{q}}$ is the radius of the target disk. The argument of $\sin(\phi - \theta_{\mathbf{q}} - \alpha)$ is small when \mathbf{q} is large so we can expand the sine and get

$$R_{\mathbf{q}} \sin \beta_{\mathbf{q}} - R \sin \alpha = q(\phi - \theta_{\mathbf{q}} - \alpha) \quad . \quad (69)$$

It is easy to see that only disks represented by coprime lattice vectors are accessible. In ref. [33] we showed that any coprime lattice vector \mathbf{q} can uniquely be written on the form $\mathbf{q} = \mathbf{q}' + n\mathbf{q}_c$, where $n \geq 2$ and \mathbf{q}' represents the lattice points closest to the line from $(0, 0)$ to \mathbf{q}_c . We say that disk \mathbf{q} lies in the \mathbf{q}_c *corridor*, see fig 4.

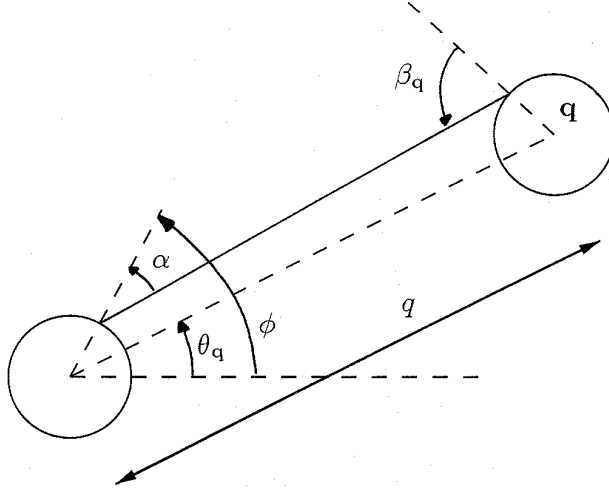


Figure 3: Definition of various angles associated with scattering to disk \mathbf{q} .

Actually there are two such neighboring lattice points for each corridor vector \mathbf{q}_c , one with smaller and one with larger polar angle. Below we assume that \mathbf{q}' is the one with the larger polar angle, the other case is completely analogous, and is accounted for by multiplying by a factor of two on some strategic occasions, see below.

The disk under observation, \mathbf{q} , is potentially shadowed only by two disks, namely $\mathbf{q} - \mathbf{q}_c$ and \mathbf{q}_c , see fig. 4. We implement the weight $w(x_s)$ by simply inflating these two disks from radius R to $(1 + \epsilon)R$.

To see how $\Omega_{\mathbf{q}_c}$ shadows $\Omega_{\mathbf{q}}$ we replace \mathbf{q} in (69) by \mathbf{q}_c and put

$$\begin{aligned} \beta_{\mathbf{q}_c} &= \pi/2 \\ R_{\mathbf{q}_c} &= (1 + \epsilon)R \\ \theta_{\mathbf{q}_c} &= \theta_{\mathbf{q}} - 1/(q q_c) \end{aligned} \quad . \quad (70)$$

This gives an equation (in terms of phase space variables α and ϕ) for the relevant boundary of $\Omega_{\mathbf{q}_c}$

$$(1 + \epsilon)R - R \sin \alpha = q_c \left((\phi - \theta_{\mathbf{q}} + \frac{1}{q q_c} - \alpha) \right) \quad . \quad (71)$$

We can now treat $\Omega_{\mathbf{q}-\mathbf{q}_c}$ in the same way. We replace \mathbf{q} in (69) by $\mathbf{q} - \mathbf{q}_c$ and put

$$\begin{aligned} \beta_{\mathbf{q}-\mathbf{q}_c} &= -\pi/2 \\ R_{\mathbf{q}-\mathbf{q}_c} &= (1 + \epsilon)R \\ \theta_{\mathbf{q}-\mathbf{q}_c} &= \theta_{\mathbf{q}} + 1/(q q_c) \end{aligned} \quad , \quad (72)$$

and get the equation for the borderline of $\Omega_{\mathbf{q}-\mathbf{q}_c}$

$$-(1 + \epsilon)R - R \sin \alpha = (q - q_c) \left((\phi - \theta_{\mathbf{q}} - \frac{1}{q q_c} - \alpha) \right) \quad . \quad (73)$$

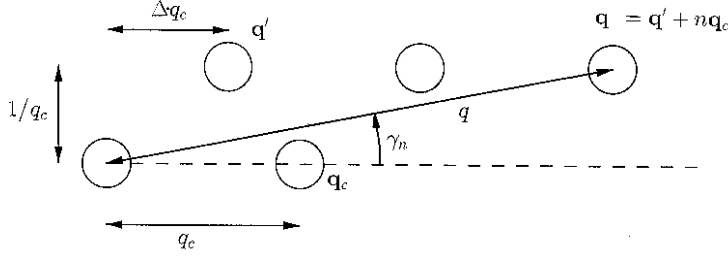


Figure 4: Scattering to disk $\mathbf{q} = \mathbf{q}' + n\mathbf{q}_c$ with $n = 2$ in the corridor \mathbf{q}_c .

Next we want to change variables from (α, ϕ) to $(\sin \alpha, \sin \beta_{\mathbf{q}})$, the relation is given by eq (69).

By combining equation (69) and (71) we see that the shadowing of $\Omega_{\mathbf{q}_c}$ corresponds to the straight line

$$q_c \sin \beta_{\mathbf{q}} + (q_n - q_c) \sin \alpha = q(1 + \epsilon) - \frac{1}{R} . \quad (74)$$

Similarly, by combining equation (69) and (73) we see that the shadowing of $\Omega_{\mathbf{q}-\mathbf{q}_c}$ is given by

$$(q - q_c) \sin \beta_{\mathbf{q}} + q_c \sin \alpha = q(1 + \epsilon) - \frac{1}{R} . \quad (75)$$

If \mathbf{q} were not shadowed, $\Omega_{\mathbf{q}}$ would be given by $-1 < \sin \beta_{\mathbf{q}} < 1$ and $-1 < \sin \alpha < 1$. So the integral (66) is simply the area of the remainder of this square, lying inside the lines given by eqs. (74) and (75).

The integration element dx_s in (66) over $\Omega_{\mathbf{q}}$ is (to leading order)

$$dx_s = \frac{R}{4\pi q} d(\sin \alpha) d(\sin \beta_{\mathbf{q}}) . \quad (76)$$

It is normalized in such a way that the integral over one octant of the plane is unity.

So we arrive at the following results

$$\hat{a}_{\mathbf{q}}(\epsilon) = \frac{R}{\pi q} \cdot \begin{cases} 1 & 0 < q < \frac{1}{2R} \frac{1}{1+\epsilon/2} \\ (1 - \frac{(1/2R - q - \epsilon q/2)^2}{q_c(q - q_c)}) & \frac{1}{2R} \frac{1}{1+\epsilon/2} < q < (\frac{1}{2R} + q_c) \frac{1}{1+\epsilon/2} \\ \frac{(1/2R - q_c - \epsilon q/2)^2}{(q - q_c)(q - 2q_c)} & (\frac{1}{2R} + q_c) \frac{1}{1+\epsilon/2} < q < \frac{2}{\epsilon} (\frac{1}{2R} - q_c) \\ 0 & \frac{2}{\epsilon} (\frac{1}{2R} - q_c) < q \end{cases} \quad (77)$$

The result can be described in the following way. All disks inside a radius $q < \frac{1}{2R} \frac{1}{1+\epsilon/2}$ are unshadowed and the corresponding trajectory segments not diffractive. Outside this horizon the accessible disks are aligned along corridors, each corridor characterized by the vector \mathbf{q}_c , subject to the condition $q_c < \frac{1}{2R} \frac{1}{1+\epsilon/2}$. Segments longer than $\frac{2}{\epsilon} (\frac{1}{2R} - q_c)$ in a particular corridor \mathbf{q}_c are always affected by diffraction. Segments longer than $\frac{2}{\epsilon} \frac{1}{2R}$ are always diffractive.

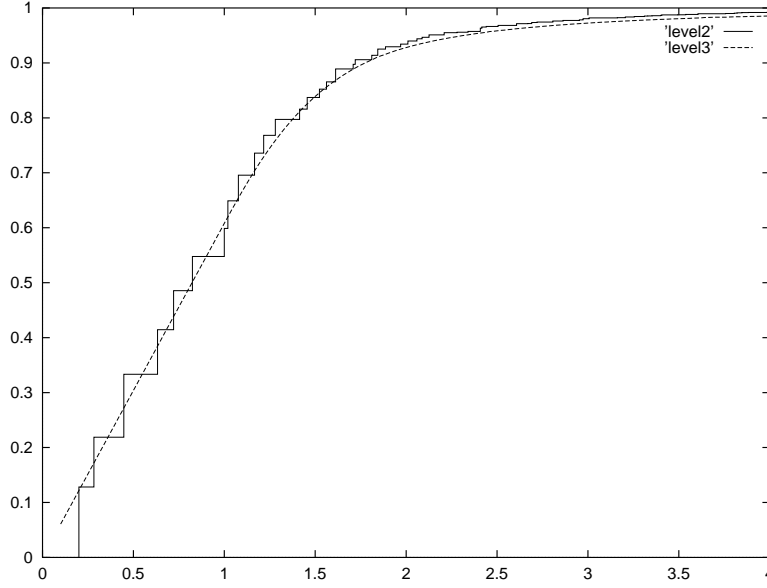


Figure 5: The integral of $p(L(\xi))$ versus ξ . The radius is $R = 0.1$ and $\epsilon = 0$. The (full) staircase curve is obtained from eq. (65) with amplitudes $\hat{a}_{\mathbf{q}}(\epsilon)$ given by (77). The (dashed) smooth curve is obtained from eq. (87,88,89).

This means that there is a one to one correspondence between corridors (beyond the horizon) and accessible disks inside the horizon, so in order to perform the sum (67) we just need to know the finite number of coprime lattice points inside the horizon, exactly how the sum should administrated we be clear below.

We can now obtain an approximate zeta function by plugging these \hat{a}_q 's into (67). The integrated recurrence time distribution $\int_0^L p(L')dL' = \sum_{\mathbf{q}:|\mathbf{q}|<L} \hat{a}_{\mathbf{q}}$ is plotted in figs. 5 and 6.

However, if R is small, there is a vast number of of coprime lattice points inside the horizon, and according to number theory, they tend to be uniformly distributed over the plane. As a matter of fact, one can use this uniformity to turn the sum into an integral and write down explicit formula for the distribution of recurrence times (65).

Asymptotically, there are $6L^2/\pi$ coprime lattice points \mathbf{q} such that $|\mathbf{q}| < L$ in the first octant so that the mean density of coprime lattice points is in an asymptotic sense

$$d_c(L) = \frac{12L}{\pi} . \quad (78)$$

(i) First we consider the case $L < \frac{1}{2R} \frac{1}{1+\epsilon/2}$.

Then $\hat{a}_{\mathbf{q}}$ is a function of q only, cf. eq. (77). The distribution function $p(L; \epsilon)$ becomes

$$p(L; \epsilon) = \sum_{\mathbf{q}} \hat{a}_{\mathbf{q}} \delta_{\sigma}(L - q) = \sum_{\mathbf{q}} \frac{R}{\pi q} \delta_{\sigma}(L - q)$$

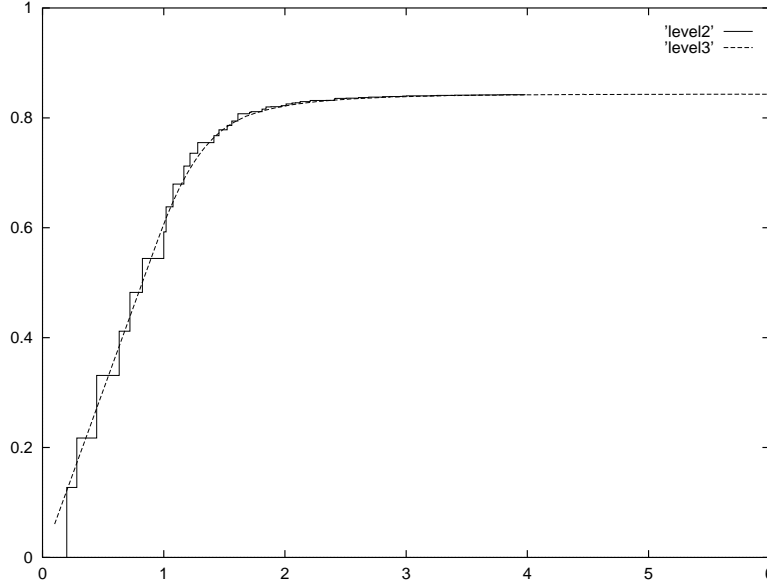


Figure 6: Same as fig. 5 but with $\epsilon = 0.2$.

$$= d_c(L) \frac{R}{\pi L} = \frac{12R}{\pi^2} . \quad (79)$$

We introduce the rescaled length $\xi = 2RL$ and rewrite

$$p(L(\xi); \epsilon) = \frac{12R}{\pi^2} \quad \xi < \frac{1}{1 + \epsilon/2} . \quad (80)$$

(ii) Next we consider the *transition region* $1/2R < L < 1/R$.

According to eq. (77) the amplitudes $\hat{a}_{\mathbf{q}}$ depend on the size of corridor $q_c = |\mathbf{q}_c|$ and the length of \mathbf{q} : $\hat{a}_{\mathbf{q}} = \hat{a}(q_c, q)$. The length q is approximately $q \approx q' + nq_c \equiv \Delta q_c + nq_c$, where Δ is a number such that $0 < \Delta < 1$, see fig 4. We get

$$\begin{aligned} p(L; \epsilon) &= 2 \sum_{\mathbf{q}_c} \sum_{n=2}^{\infty} \hat{a}(q_c, q) \delta_{\sigma}(L - q) \\ &= 2 \sum_{\mathbf{q}_c} \sum_{n=2}^{\infty} \hat{a}(q_c, q) \delta_{\sigma}(L - q_c n - \Delta q_c) , \end{aligned} \quad (81)$$

where we inserted the factor 2 to account for both neighbors of \mathbf{q}_c .

We will now turn the sums over \mathbf{q}_c and n into an integral over the density of coprime lattice vectors. The parameter Δ is uniformly distributed in the interval $0 < \Delta < 1$ [20], this means that we can just integrate n from $n = 2$ to ∞ .

$$p(L; \epsilon) = 2 \int_0^{1/2R - \epsilon L/2} dq_c d_c(q_c) \hat{a}(q_c, L) \int_{n=2}^{\infty} \delta_{\sigma}(L - q_c n) ,$$

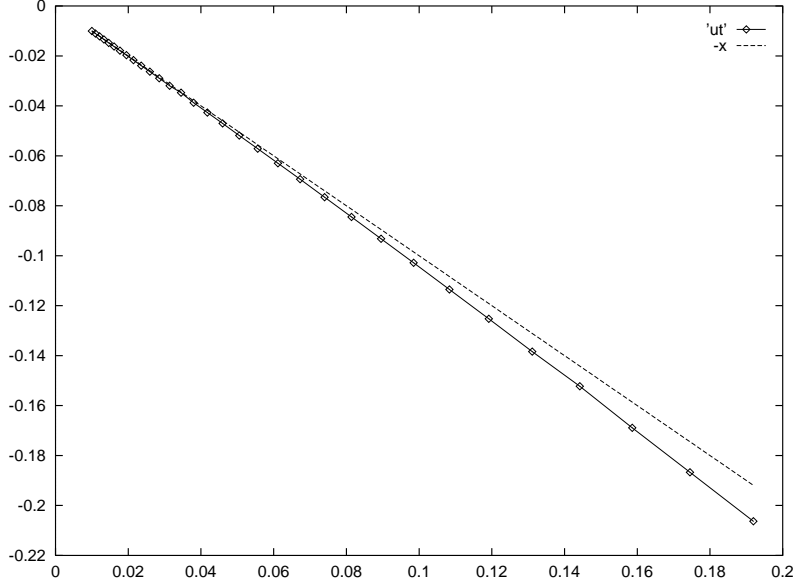


Figure 7: The leading zero $z_0(\epsilon)$ versus ϵ compared with the asymptotic formula (93).

$$\begin{aligned}
&= 2 \int_0^{1/2R-\epsilon L/2} dq_c d_c(q_c) \hat{a}(q_c, L) \frac{1}{q_c} \theta_\sigma(L - 2q_c) \\
&= 2 \int_0^{\min(1/2R-\epsilon L/2, L/2)} dq_c d_c(q_c) \hat{a}(q_c, L) \frac{1}{q_c} ,
\end{aligned} \tag{82}$$

where $\theta(x)$ is the unit step function.

Since we are considering the region $\frac{1}{2R} \frac{1}{1+\epsilon/2} < q < \frac{1}{R} \frac{1}{1+\epsilon}$, we have $\min(1/2R - \epsilon L/2, L/2) = L/2$. Next we insert the expression for $\hat{a}(q_c, q)$ from eqs. (77) and $d_c(q_c)$ from eq. (78)

$$\begin{aligned}
p(L; \epsilon) &= 2 \int_{l+\epsilon L/2-1/2R}^{l/2} dq_c \frac{12q_c}{\pi} \frac{1}{q_c} \frac{R}{\pi L} \left(1 - \frac{(1/2R - L - \epsilon L/2)^2}{q_c(L - q_c)}\right) \\
&\quad + 2 \int_0^{L-\epsilon L/2-1/2R} dq_c \frac{12q_c}{\pi} \frac{1}{q_c} \frac{R}{\pi L} \frac{(1/2R - q_c - \epsilon L/2)^2}{(L - q_c)(l - 2q_c)} .
\end{aligned} \tag{83}$$

We change integration variable to $\eta = 2Rq_c$ and use as before $\xi = 2RL$. This leaves us the following integral to solve

$$p(L(\xi); \epsilon) = \frac{24R}{\pi^2} \left(\int_{\xi+\epsilon\xi/2-1}^{\xi/2} \frac{d\eta}{\xi} \left(1 - \frac{(1 - \xi - \epsilon\xi/2)^2}{\eta(\xi - \eta)}\right) + \int_0^{\xi+\epsilon\xi/2-1} \frac{d\eta}{\xi} \frac{(1 - \eta - \epsilon\xi/2)^2}{(\xi - \eta)(\xi - 2\eta)} \right) . \tag{84}$$

The result of this integral is displayed below (88).

(iii) Now remains only the case $\frac{1}{R} \frac{1}{1+\epsilon} < L < \frac{2}{\epsilon}$:

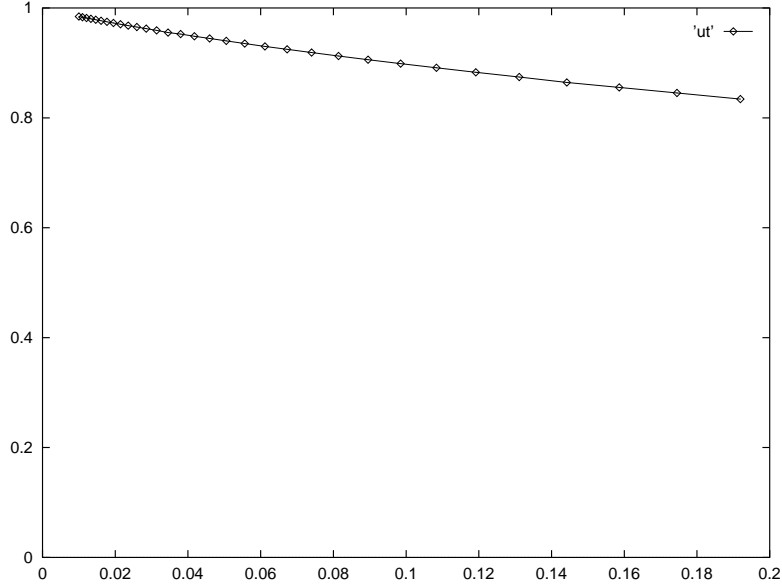


Figure 8: The derivative $\hat{Z}'(z_0)$ evaluated at the leading zero versus ϵ . It approached unity as $\epsilon \rightarrow 0$ as predicted by eq. (94).

The calculation is completely analogous to the previous case and we get

$$\begin{aligned}
p(L(\xi); \epsilon) &= 2 \int_0^{1/2R - \epsilon L/2} dq_c d_c(q_c) \frac{1}{q_c} a(q_c, q = L) \\
&= 2 \int_0^{1/2R - \epsilon L/2} dq_c \frac{12q_c}{\pi} \frac{1}{q_c} \frac{R}{\pi L} \frac{(1/2R - q_c - \epsilon L/2)^2}{(L - q_c)(L - 2q_c)} \\
&= \frac{24R}{\pi^2} \int_0^{1 - \epsilon\xi/2} \frac{d\eta}{\xi} \frac{(1 - \eta - \epsilon\xi/2)^2}{(\xi - \eta)(\xi - 2\eta)} .
\end{aligned} \tag{85}$$

It is time to summarize the results. It is natural to display the final results in terms of the distribution of the rescaled recurrence lengths ξ rather than L . We call the distribution $f(\xi; \epsilon)$ and it is trivially related to $p(L; \epsilon)$ according to

$$p(L; \epsilon)dL = f(\xi; \epsilon)d\xi . \tag{86}$$

Inside the horizon we already have

$$f(\xi; \epsilon) = \frac{6}{\pi^2} \quad \xi < \frac{1}{1 + \epsilon/2} \tag{87}$$

Beyond the horizon we get, after having performed the integrals (84) and (85) ²

$$\begin{aligned}
f(\xi; \epsilon) &= \frac{3}{\pi^2 \xi^2} (2\xi - \epsilon\xi^2 + [4\xi - 3\xi^2 - 2\epsilon\xi^2] \log \xi + \\
&\quad [4\xi^2 - 8\xi^2 + 4 - 4\epsilon\xi^2 - \epsilon^2\xi^2 - 4\epsilon\xi] \log(\xi(1 + \epsilon/2) - 1) \\
&\quad + [4\xi - \xi^2 - 4 - 2\epsilon\xi^2 - \epsilon^2\xi^2 + 4\epsilon\xi] \log |\xi(1 + \epsilon) - 2|) \quad \frac{1}{1 + \epsilon/2} < \xi < 2/\epsilon
\end{aligned} \tag{88}$$

²The results of these two integrals can be summarized in one formula, note the absolute value in one of the logarithms

This is valid up to the point $\xi = 2/\epsilon$ where the function chokes. After that we have

$$f(\xi; \epsilon) = 0 \quad 2/\epsilon < \xi \quad . \quad (89)$$

The integral $\int_0^\xi f(\xi'; \epsilon) d\xi'$ if these expressions is plotted in figs. 5 and 6. We note that the statistical treatment of the lattice vectors works surprisingly well, even for such a "large" radius as $R = 0.1$.

It is also natural to let the zeta functions depend on a rescaled variable z as defined by

$$s = 2Rz \quad . \quad (90)$$

A power series expansion of the the zeta function is related to the moments of the distribution $f(\xi; \epsilon)$

$$\hat{Z}(z; \epsilon) = 1 - \int e^{-z\xi} f(\xi; \epsilon) d\xi = 1 - \sum_{m=0}^{\infty} \frac{(-z)^m}{m!} \int \xi^m f(\xi; \epsilon) d\xi \quad , \quad (91)$$

These moments can be computed from eqs. (87),(88) and (89) and are found to be

$$\int \xi^m f(\xi; \epsilon) d\xi = \begin{cases} 1 - \epsilon + O(\epsilon^2 \log \epsilon) & m = 0 \\ (1 + O(\epsilon \log \epsilon)) & m = 1 \\ O(\log \epsilon) & m = 2 \\ O(1/\epsilon^{m-2}) & m \geq 3 \end{cases} \quad . \quad (92)$$

The leading zero z_0 of the zeta function can be computed from eqs. (91) and (92), and is found to be

$$z_0 = -\epsilon + O(\epsilon^2 \log \epsilon) \quad . \quad (93)$$

We are also interested in the derivative of the zeta function evaluated at at this zero

$$\hat{Z}'(z_0) = 1 + O(\epsilon \log \epsilon) \quad . \quad (94)$$

In figs. 7 and 8 we compare these asymptotic formulas with results from numerical computation of the BER zeta function as obtained from eqs. (87),(88) and (89).

Traces will not be a direct concern to us. But, by computing traces in the BER framework, we can get an idea of the influence of non leading zeros by computing the trace in the BER approximation. That information is relevant for the next section. The computation is done numerically by FFT technique.

The trace formula is in our rescaled units

$$tr \mathcal{L}_\epsilon^\xi = \frac{1}{2\pi i} \int_{a-i\infty}^{a+i\infty} e^{z\xi} \frac{d}{dz} \log \hat{Z}_w(z) dz \quad . \quad (95)$$

Traces for $\epsilon = 0$ and $\epsilon = 0.1$ are plotted in figs. 9 and 10. For small ξ the trace (in the BER approximation) is given by

$$tr \mathcal{L}_\epsilon^\xi = \exp(6\xi/\pi^2) - 1 \quad \xi < \frac{1}{1 + \epsilon/2} \quad . \quad (96)$$

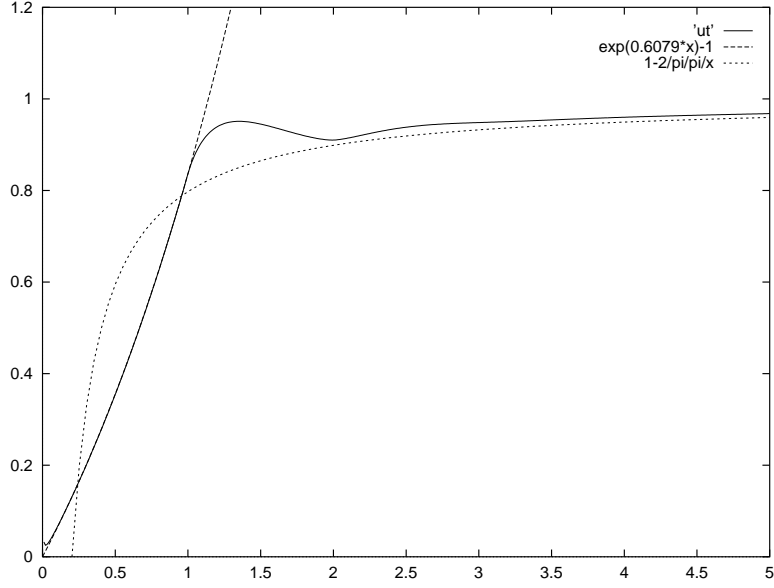


Figure 9: The trace (95) for $\epsilon = 0$ (full line). Comparison is made with eq. (96) for small values of ξ (dashed line) and eq. (98) for large values of ξ (dotted line).

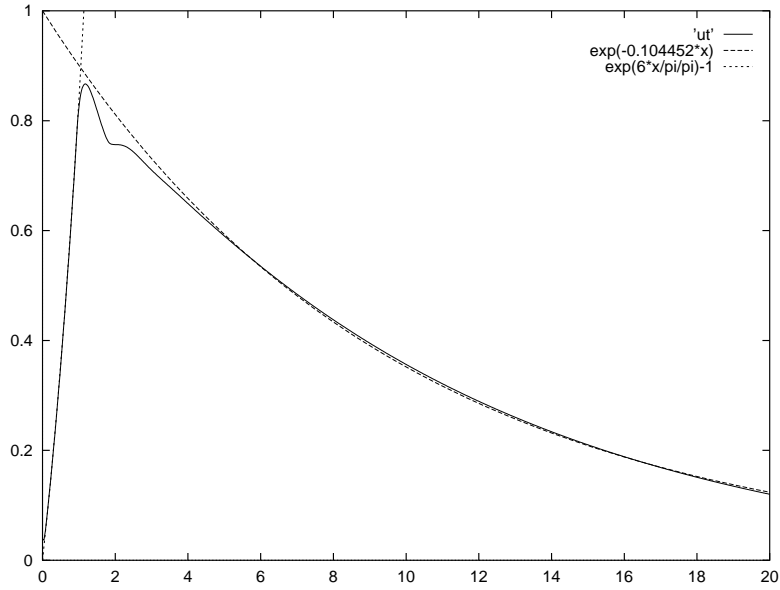


Figure 10: The trace (95) for $\epsilon = 0.1$. Comparison is made with eq. (96) for small values of ξ (dotted line) and eq. (97) for large values of ξ (dashed line).

If the reader want to verify this, the following hint should be useful: The trace $tr\mathcal{L}_\epsilon^\xi$ in the range $\xi < \Xi$ depends only on the behavior of the distribution $f(\xi)$ in the same range ($\xi < \Xi$) and f is constant in this range.

In the large ξ limit, the asymptotic behavior is given by the leading zero z_0 , and thus

$$tr\mathcal{L}_\epsilon^\xi \sim \exp(z_0\xi) \sim \exp(-\epsilon\xi) \quad , \quad (97)$$

see fig 10. We observe that this asymptotic result settles down very early, that is long before the natural scale $2/\epsilon$, cf. eq. (89).

For any finite ϵ the zeta function is entire since $p(L)$ has compact support. But when $\epsilon \rightarrow 0$ zeros will accumulate along the negative real z - axis, building up a branch cut. For the limiting case $\epsilon = 0$ this will lead to a power law correction

$$tr\mathcal{L}^\xi \sim 1 - \frac{2}{\pi^2\xi} \quad , \quad (98)$$

see fig 9. This power law will not be essential in the following.

We also need to know the value of $Z_2(z_0; \epsilon)$ as defined in (61). This zeta function contain the square of $|\Lambda_p|$ in the denominator. This means that at $z = z_0$ (which is close to the origin for small ϵ) the value of the zeta function will be dominated by the shortest cycles, which, for small ϵ , will be non diffractive. This implies that $Z_2(z_0; \epsilon)$ tends to a constant faster than $\hat{Z}'(z_0)$ do, as $\epsilon \rightarrow 0$. A simple estimate, based on the methods in [22] suggests that

$$Z_2(z_0, \epsilon) = 1 + O(R^2 \log R) + O(R^2)O(\epsilon) \quad (99)$$

which should be compared with eq. (94).

4 Results

We now possess all the tools we need to finally be able to compute the asymptotic limit of the error estimate F . To obtain this we fetch from section 3.2

$$F = \sqrt{1 - \frac{\int_0^{\xi_{BK}} b(\xi; \epsilon) d\xi}{\int_0^{\xi_{BK}} b(\xi; 0) d\xi}} \quad , \quad (100)$$

where

$$\xi_{BK} = 2RL_{BK} = A kR \quad , \quad (101)$$

cf eq. (14). To begin with we are only interested in the leading asymptotic behavior of the function $b(\xi; \epsilon)$. From section 3.2 we therefore collect

$$b(\xi; \epsilon) \sim \frac{Z_2(z_0; \epsilon)}{Z'(z_0; \epsilon)} e^{z_0\xi} \quad , \quad (102)$$

valid for large values of ξ . From section 3.3 we find

$$z_0 \sim -\epsilon \quad (103)$$

$$Z'(z_0; \epsilon) \sim 1 \quad (104)$$

$$Z_2(z_0; \epsilon) \sim Z_2(0, 0) \quad (105)$$

to leading order in ϵ , for error bounds please go back to section 3.3. Finally, from section 2.5 we have

$$\epsilon = c(kR)^{-2/3} \quad (106)$$

We are then in the position to compute the large kR limit of the error estimate, which we easily evaluate to

$$F \sim \left(1 - \frac{1 - e^{-\epsilon \xi_{BK}}}{\epsilon \xi_{BK}}\right)^{1/2} = \left(1 - \frac{1 - e^{-cA(kR)^{1/3}}}{cA(kR)^{1/3}}\right)^{1/2} \quad (107)$$

We observe that this function will definitely approach unity which implies that individual eigenstates ceases to be resolved. This final collapse will occur on the scale

$$kR \sim (cA)^{-3} \quad (108)$$

Note that if only one symmetry subspace is considered, then $A \approx 1/8$, so this might correspond to a very high energy.

But how is this asymptotic expression approached.

Actually we know that $F = 0$ if kR is less than some critical value which is given by $\xi_{BK} = 1/(1 + \epsilon/2)$ (cf. eq. (96)) or written out explicitly

$$A kR = \frac{1}{1 + \frac{\epsilon}{2}(kR)^{-2/3}} \quad (109)$$

The solution is given by

$$(kR)_{threshold} = \left(\frac{1}{6}\alpha^{1/3} - c \alpha^{-1/3}\right)^3, \quad (110)$$

where

$$\alpha = \frac{108}{A} + 6\sqrt{6c^3 + 324/A^2} \quad (111)$$

Unstable periodic orbit below this threshold are never diffractive. Of course, neutral orbits in this range are subject to diffraction corrections but we do only consider the error due to unstable orbits. We are thus unable to estimate the semiclassical error for small values of kR .

To estimate the intermediate behavior we introduce a further approximation of eq. (59)

$$b(\xi; \epsilon) = \frac{1}{2\pi i} \int_{\sigma-i\infty}^{\sigma+i\infty} \frac{Z_2(z; \epsilon)}{Z(z; \epsilon)} e^{z\xi} dz \approx Z_2(0, 0) \int_{\sigma-i\infty}^{\sigma+i\infty} \frac{1}{Z(z; \epsilon)} e^{z\xi} dz \quad (112)$$

which is highly reasonable, cf. eq. (99) . We replace the classical zeta function $Z(z, \epsilon)$ by the approximate one $\hat{Z}(z, \epsilon)$, the transforms are again computed by FFT technique and the resulting function $F(kR)$ is plotted in fig. 11. In the computation we use

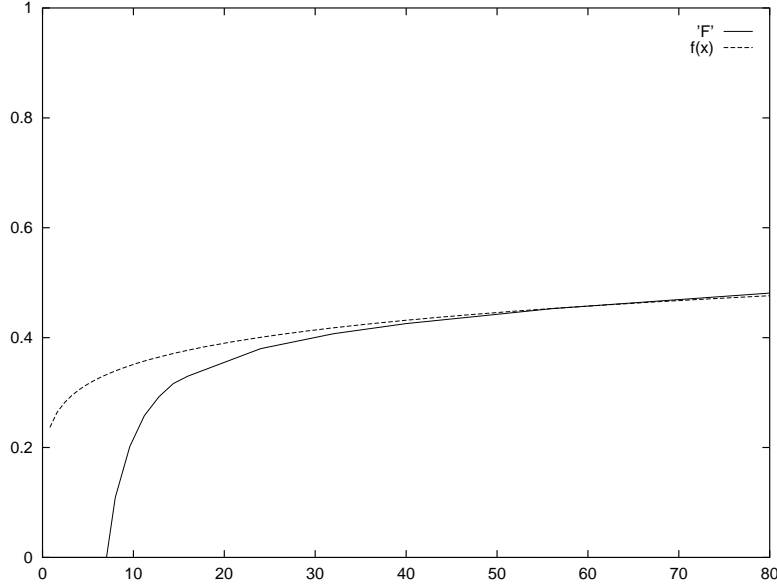


Figure 11: The error estimate $F(kR)$ versus kR according to eqs (112) (full line) compared with the asymptotic expression (100) (dashed line). $A = 1/8$ and c is chosen to be $c = 1$.

$A = 1/8$ and an arbitrary value of $c = 1$. We see is a very steep ascent at the threshold discussed above and a fast approach to the asymptotic formula (107). It is likely that the individual states ceases to be resolved already here. However, it is hard to make any safe prediction regarding the crudeness of our treatment of the penumbra problem, see also the discussion of c below. However, the function F *does* approach unity, sooner or later, and it is difficult to find an prevarication of this fact.

There is an issue which we appear to have forgotten, the constant c in eq. (127) is not really a constant, it depends weakly on kR , R , r_1 and r_2 , see fig 1 and appendix A. First, this dependence is too weak to be able to alter our general conclusions. Moreover, it is not obvious how to implement the dependence on r_1 and r_2 . In the BER application we consider disk to disk segment whereas in the study of the circle Green function in sec 2.5 we consider (square) boundary to boundary segments. To make the exact connection one has to convolute the Circle Green function with itself, the outcome of this operation is not obvious. So we used c as if it was a constant when implementing the BER approximation. Therefore the "constant" c coming out of the other end of the BER calculation should have some residual weak dependence on R and kR .

5 Discussion of the validity of the various approximations involved

No chain is stronger than the weakest link. The results presented here is based on a long series of approximations and assumptions. Some of them may be readily justified and should hardly be controversial but some may seem a lot more crude and one may ask if they will allow the chain to break.

5.1 The correction to the semiclassical weights

On one hand we argued that penumbra diffraction cannot be accounted for by multiplicative corrections but on the other hand we *needed* multiplicative corrections to be able to use the machinery of the periodic orbit theory and evolution operators. So we simply constructed a multiplicative weight inspired by the penumbra diffraction that should be able to provide us with an estimate of the error in the Berry-Keating formula. The procedure was discussed at some length in sec. 2.5.

One could object that it is too crude to approximate the gradual transition of the circle Green function with a step function, and suggest a more smooth weight. This is in principle possible, but that would make the calculation in sec. 3.3 immensely more complicated without changing the result in any significant way.

5.2 The BER approximation

It is natural that a theory for the asymptotics of the periodic orbits is hard to check numerically. In ref. [20] we compared the exact trace formulas with those of the BER approximation for lengths up to roughly the horizon $1/2R$ for the Sinai billiard. The results were encouraging but hardly asymptotic.

However, a range of asymptotic predictions of the BER approximation appears to be correct. It does provide the suggested exact diffusion behavior in the regular Lorentz gas (with unbounded horizon) [34, 22] and the related correlation decays [35] as well as the small radius limit of the Lyapunov exponent[33]. We therefore feel confident that the approach works even if more rigorous results are called for.

We introduced some extra approximations, valid in the small R limit, but our experience is that they work excellent even for rather large R .

One could again raise objection that the diffractive weight is discontinuous and that this could cause problems for averages to settle down. But we saw in section 3.3 that the effect is just to change the pruning rules slightly, the billiard is as discontinuous as before and the fluctuations of the pseudo orbit sums appearing in the numerator and denominator (60) are similar. The integrals in eq. (60) are self averaging and the fluctuations of the integrands irrelevant for the estimate of the error.

5.3 The diagonal approximation

The diagonal approximation underlying eq. (46) can be verified assuming that the spectral statistics is given by Random Matrix Theories [36]. The diagonal approximation

on the diffractive sum behind (47) is natural, in particular since the majority of pseudo orbits are diffractive for small ϵ , but by no means obvious.

I am grateful to Jon Keating for a very useful discussion. This work was supported by the Swedish Natural Science Research Council (NFR) under contract no. F-AA/FU 06420-313.

A Stationary phase analysis of the circle Green function

We will consider scatterings in extreme forward angles so only the second term in the integral (35) ($m=0$) contributes. This means that we only need to evaluate the integral

$$G^{(0)}(r_1, r_2, \Delta\theta) = \frac{i}{8} \int_{-\infty}^{\infty} S_\ell(kR) H_\ell^{(1)}(kr_1) H_\ell^{(1)}(kr_2) e^{i\ell\Delta\theta} d\ell \quad , \quad (113)$$

where $0 \ll \Delta\theta < \pi$. Actually, this integral is divergent but as long as we study the stationary phase approximation, it serves our purposes. We can still safely use the Debye approximation for the Hankel functions $H_\ell^+(kr_1)$ and $H_\ell^+(kr_2)$

$$H_\ell^{(1)}(z) \sim \sqrt{\frac{2}{\pi\sqrt{z^2 - \ell^2}}} e^{i[\sqrt{z^2 - \ell^2} - \ell \arccos(\ell/z) - \pi/4]} \quad , \quad (114)$$

because $kr_1 \gg \ell$ and $kr_2 \gg \ell$. However, the phase shift function needs a more careful analysis. The phase shift function $S_\ell(kR)$ is of unit modulus and we call the phase $\gamma(kR, \ell)$

$$S_\ell(kR) = -\frac{H_\ell^{(2)}(kR)}{H_\ell^{(1)}(kR)} \equiv e^{i\gamma(kR, \ell)} \quad . \quad (115)$$

The Green function now reads

$$G^{(0)}(r_1, r_2, \Delta\theta) = \int_{-\infty}^{\infty} A(r_1, r_2) e^{i(\ell\Delta\theta - \Psi(\ell))} d\ell \quad , \quad (116)$$

where the slowly varying amplitude $A(r_1, r_2)$ is composed of the Hankel functions $H_\ell^{(1)}(kr_1)$ and $H_\ell^{(1)}(kr_2)$. The asymptotics of the integral is determined by the phase function

$$\Psi(\ell) = -\gamma(kR, \ell) - [\sqrt{(kr_1)^2 - \ell^2} - \ell \arccos(\ell/(kr_1))] - [\sqrt{(kr_2)^2 - \ell^2} - \ell \arccos(\ell/(kr_2))] + \pi/2 \quad . \quad (117)$$

We will now investigate the phase of $S_\ell(kR)$ in detail. To this end we will use the uniform approximation for Hankel functions relating the phase of Hankel functions to the phase of Airy functions according to [37]

$$S_\ell(kR) = -\frac{\text{Ai}(-x) + i\text{Bi}(-x)}{\text{Ai}(-x) - i\text{Bi}(-x)} \equiv e^{i\gamma(\ell, kR)} \quad , \quad (118)$$

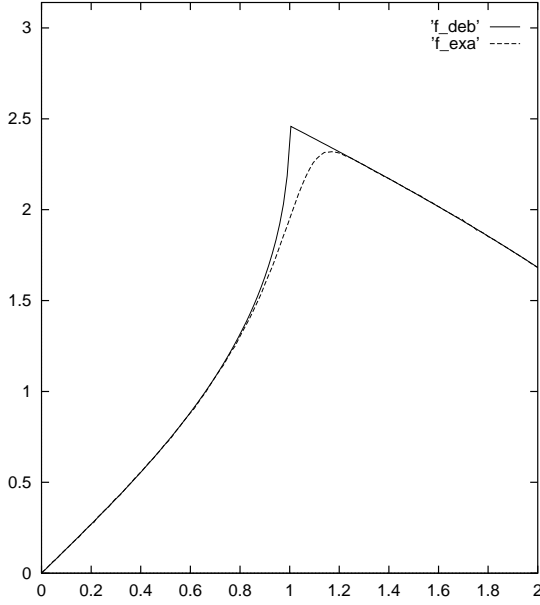


Figure 12: The function $\Psi_\ell(\ell)$ versus ℓ for fixed values of $k = 30$, $R = 1$ and $r_1 = r_2 = 3$

where

$$x(kR, \ell) = \begin{cases} \left[\frac{3}{2}(\sqrt{(kR)^2 - \ell^2} - \ell \arccos(\ell/(kR))) \right]^{2/3} & \ell < kR \\ -\left[\frac{3}{2}(\ell \cdot \log(\frac{\ell + \sqrt{\ell^2 - (kR)^2}}{kR}) - \sqrt{\ell^2 - (kR)^2}) \right]^{2/3} & \ell > kR \end{cases} . \quad (119)$$

Defining

$$\ell = kR(1 + \epsilon) , \quad (120)$$

we have for small ϵ

$$-x = (\sqrt{2}kR)^{2/3}(\epsilon + O(\epsilon^2)) . \quad (121)$$

Using this expression for x one gets the so called transition region approximation. This approximation fails to yield the Debye approximation as its asymptotic limit but the nice thing is that there is a considerable overlap because whenever $x \ll \ell^{2/3}$ we can use the transition region approximation and when $x \gg 1$ we can use Debye.

$\gamma(x)$ is a complicated function but one has the following asymptotic expressions [37]

$$\gamma(x) \sim -e^{-\frac{4}{3}(-x)^{3/2}}(1 + O(1/(-x)^{3/2})) \quad x \rightarrow -\infty , \quad (122)$$

$$\gamma(x) = -\frac{\pi}{2} - \frac{4}{3}x^{3/2} + O(x^{-3/2}) \quad x \rightarrow +\infty , \quad (123)$$

so we obtain the Debye approximation when $x \rightarrow \infty$ as expected.

The stationary phase condition will simply read $\Psi_\ell(\ell) = \Delta\theta$ (subscripts denote differentiation). In fig. 12 we plot the function $\Psi_\ell(\ell)$ versus ℓ for some arbitrary chosen values of $r_1/R = r_2/R = 3$ and $kR = 30$ together with its Debye approximation. The plot gives a picture of how the stationary phase will perform for all $\Delta\theta$, just place the

ruler horizontally at $\Delta\theta$. If it goes below the maximum, it intersects the curve twice. The corresponding saddle points corresponds to the direct (larger ℓ) and reflected ray (smaller ℓ) respectively.

We are interested in the location of the maximum of $\Psi_\ell(\ell)$. This turns out the lie in the region where eqs (121) *and* (122) applies. To leading order in (kR) the location of the maximum is the solution to the equation

$$-xe^{-\frac{4}{3}(-x)^{3/2}} = 2^{-8/3}(kR)^{-1/3} \left(\frac{R}{\sqrt{r_1^2 - R^2}} + \frac{R}{\sqrt{r_2^2 - R^2}} \right) \equiv (kR)^{-1/3} C(r_1, r_2) . \quad (124)$$

By elementary methods one can show that the solution to this equation lies in the range

$$\frac{9}{16} \left(\log \frac{(kR)^{1/3}}{C(r_1, r_2)} \right)^{2/3} < (-x)_{max} < \left(\log \frac{(kR)^{1/3}}{C(r_1, r_2)} \right)^{2/3} . \quad (125)$$

Where in this range the solution lies is completely irrelevant for us. We use this liberty and choose ϵ in (36) to be (cf. eq. (121))

$$\epsilon_{max} = 2^{-1/3}(kR)^{-2/3} \left(\log \frac{(kR)^{1/3}}{C(r_1, r_2)} \right)^{2/3} \equiv c(kR)^{-2/3} . \quad (126)$$

where

$$c = c(kR, R, r_1, r_2) = 2^{-1/3} \left(\frac{1}{3} \log kR + \frac{8}{3} \log 2 - \log \left(\frac{R}{\sqrt{r_1^2 - R^2}} + \frac{R}{\sqrt{r_2^2 - R^2}} \right) \right)^{2/3} \quad (127)$$

References

- [1] M. C. Gutzwiller, *Chaos in Classical and Quantum Mechanics*, Springer, New York (1990).
- [2] E. J. Heller, S. Tomsovic and M. A. Sepéveda, *Chaos* **2**, 105 (1992).
- [3] M. V. Berry and J. P. Keating, *J. Phys. A* **23**, 4839 (1990)
- [4] P. Cvitanović and B. Eckhardt, *Phys. Rev. Lett.* **63**, 823 (1989). (1993).
- [5] P. A. Boasman, *Nonlinearity* **7**, 485 (1994).
- [6] E. B. Bogomolny, *Nonlinearity* **5**, 805 (1992).
- [7] P. Dahlqvist, *J. Phys. A* **24**, 4763 (1991).
- [8] F. Christiansen and P. Cvitanović, *Chaos* **2**, 61 (1992).
- [9] G. Tanner, P. Scherer, E. B. Bogomolny, B. Eckhardt and D. Wintgen, *Phys. Rev. Lett.* **67** 2410 (1991).

- [10] M. Sieber and F. Steiner, Phys. Rev. Lett. **67**, 1941 (1991).
- [11] H. Primack and U. Smilansky, J. Phys. A **31**, 6253 (1998).
- [12] M. Saraceno and A. Voros, Chaos **2**, 99 (1992).
- [13] B. Sundaram and R. Scharf, Physica D **83**, 257 (1995).
- [14] M. Sieber, N. Pavloff and C. Schmit, Phys. Rev. E **55**, 2279 (1997).
- [15] H. Schomerus and M. Sieber, J. Phys. A **30**, 4537 (1997).
- [16] G. Tanner, J. Phys. A **30**, 2863 (1997).
- [17] H. Primack, H. Schanz, U. Smilansky and I. Ussishkin, Phys. Rev. Lett. **76**, 1615 (1996).
- [18] V. Baladi, J. P. Eckmann and D. Ruelle, Nonlinearity **2** (1989) 119.
- [19] P. Dahlqvist, J. Phys. A **27**, 763 (1994).
- [20] P. Dahlqvist, Nonlinearity **8**, 11 (1995).
- [21] P. Dahlqvist, J. Techn. Phys. **38**, 189 (1997).
- [22] P. Dahlqvist, J. Stat. Phys. **84**, 773 (1996).
- [23] J. H. Hannay and M. V. Berry, Physica D **1**, 267 (1980).
- [24] J. P. Keating, Nonlinearity **4**, 309 (1991).
- [25] M. C. Gutzwiller, Phys. Rev. Lett. **45**, 150 (1980).
- [26] P. Dahlqvist, Chaos Solitons and Fractals **8**, 1011, (1997).
- [27] P. Cvitanović et.al. *Classical and Quantum Chaos: A Cyclist Treatise*, <http://www.nbi.dk/ChaosBook/>, Niels Bohr Institute (Copenhagen 1997).
- [28] C. F. F. Karney, Physica D **8**, 360 (1983).
- [29] M. V. Berry and M. Wilkinson, Proc. R. Soc. Lond. A **A392**, 15 (1984).
- [30] B. R. Levy and J. B. Keller, Comm. Pure. Appl. Math, **12**, 159 (1959).
- [31] K. T. Hansen, *Symbolic Dynamics in Chaotic Systems*, Ph.D. thesis, Oslo (1990).
- [32] R. Artuso, E. Aurell and P. Cvitanović, Nonlinearity **3**, 325 and 361, (1990).
- [33] P. Dahlqvist, Nonlinearity **10**, 159 (1997).
- [34] P. M. Bleher, J. Stat. Phys. **66**, 315, (1992).
- [35] P. Dahlqvist, R. Artuso, Phys. Lett. A **219**, 212 (1996).
- [36] J. P. Keating, private communication.
- [37] M. Abramovitz and I. A. Stegun, *Handbook of mathematical functions*, Washington: National Bureau of Standards, (1964).